https://doi.org/10.3311/PPme.41247

Periodica Polytechnica Mechanical Engineering, 69(3), pp. 259–273, 2025

Lamé Curve-based Spiral Tool Path Generation for Rough Milling

Viktor Tancsa[1*], Adam Jacso[1], Gyorgy Poka[1]

[1] Department of Manufacturing Science and Engineering, Faculty of Mechanical Engineering, Budapest University of Technology and Economics, Műegyetem rkp. 3., H-1111 Budapest, Hungary
[*] Corresponding author, e-mail: tancsav@edu.bme.hu

Received: 11 June 2025, Accepted: 27 July 202X, Published online: 11 August 2025

Abstract

Automatic tool path generation for milling has been a subject of research for decades. The primary challenge in this area lies in simultaneously satisfying both geometric and technological constraints. Although various methods have been developed for spiral trajectory generation to meet these strict criteria, the potential of Lamé curves (also known as superellipses) has remained unexplored. This paper aims to address this gap by introducing a new algorithm that parametrises Lamé curves and transforms them into spirals using polar coordinate functions. The novel method generates a continuous tool path that smoothly fills the region between two closed boundaries without interrupting the cutting process. The algorithm was validated through case studies involving various pocket-like and island-like geometries. For the comparative analysis, two widely used strategies were selected as benchmarks: the traditional contour-parallel strategy and the advanced adaptive milling strategy. The simulation and cutting experiments conducted to analyse cutter engagement, tool load, and machining time demonstrated that the Lamé-based spiral paths achieved 1–44% improvements in machining time and 3–17% reductions in peak cutting force. These improvements are attributed to the smooth path curvature and the stable cutter engagement along the path, which enables effective tool load control. Although the strategy has certain geometric limitations, the results indicate that Lamé-based spirals offer a promising alternative for improving productivity and tool life in rough milling.

Keywords

Lamé curve, superellipse, spiral tool path, CNC machining, rough milling

1 Introduction

With the continuous advancement of manufacturing technologies, increasingly complex components with complex pockets are being produced, most of which can be machined via 2.5D milling. In the case of such closed pockets, the primary challenge lies in the often difficult accessibility of the allowance geometry, complicating the maintenance of optimal cutting conditions. Since rough machining can account for up to half or even more of the total machining time, it is essential to employ tool path strategies that not only ensure efficient material removal but also optimise tool load conditions [1, 2]. A well-chosen tool path can contribute to extended tool life, improved surface quality, and enhanced energy efficiency [3].

In practice, several clearly defined objectives assist in identifying the optimal solution:

1. reducing the number of direction changes extends tool life and reduces energy consumption,
2. avoiding sharp direction changes and linking movements improves overall machining efficiency, and
3. maintaining constant tool engagement results in longer tool life and superior surface finish [2].

This is especially critical today, where advanced technologies such as High-Speed Machining (HSM) have become standard in metal cutting, simultaneously offering increased productivity and enhanced quality. However, HSM is particularly sensitive to path continuity: sharp corners or sudden directional changes require the tool to decelerate and accelerate again, significantly increasing cycle times and potentially causing unfavourable cutting conditions. The full benefits of HSM can only be realised when the tool path is continuous, smooth, and the tool load is uniform, even if this results in longer tool paths [4, 5].

Cite this article as: Tancsa, V., Jacso, A., Poka, G. "Lamé Curve-Based Spiral Tool Path Generation for Rough Milling", Periodica Polytechnica Mechanical Engineering, 69(3), pp. 259–273, 2025. https://doi.org/10.3311/PPme.41247

To leverage these advantages, pocket machining strategies have been a major research focus for decades, yielding numerous solutions to meet the demanding requirements of tool path generation.

1.1 Controlling the tool load

Before focusing on specific tool path generation strategies, it is worth reviewing general measures that help maintain constant tool load. Ensuring a consistent tool load is important because it allows the tool to operate continuously near the maximum allowable load, thus increasing machining efficiency and tool life. Additionally, reducing load fluctuations minimises the risk of tool breakage and vibrations, and enables more precise machining [6].

The tool-workpiece engagement is characterised by the cutter engagement angle, defined as the central angle corresponding to the arc length of the tool in contact. This parameter determines the cross-sectional area of the material being removed and directly influences the tool load. To maintain a constant cutter engagement angle along the spiral tool path, a specialised spiral shape with increasing stepover is necessary [7]. However, this approach can only be applied to areas with circular boundaries. If the spiral-like tool path differs from this special shape, even a regular Archimedean spiral will result in variations in the cutter engagement at different points along the path.

There are two main approaches to managing fluctuations in tool load: feed rate control and radial depth control. For a long time, feed rate control has been used to mitigate the effects of varying cutter engagement [8]. Nowadays, several methods are available for this purpose, including geometric, cutting force model-based, and data-driven techniques [9]. In this work, a traditional geometric feed rate scheduling method based on material removal rates (MRR) was chosen.

1.2 Overview of tool path generation strategies

Traditional *direction-parallel* [10] and *contour-parallel* [11] strategies still dominate pocket milling operations. Due to their simplicity, predictability, and widespread availability, they remain the default solutions in many CAM systems. However, these strategies have numerous limitations, particularly in the context of HSM, restricting their applicability in modern manufacturing [2].

The direction-parallel strategy involves the tool moving along parallel linear passes in a predefined direction. Although simple, unidirectional scanning often requires frequent tool retracts [2], and bidirectional movement can result in a non-uniform surface due to alternating climb and conventional milling passes [12]. Additionally, fluctuations in cutter engagement along the side walls adversely affect tool load stability [13].

The contour-parallel strategy employs equidistant offset curves conforming to the boundary, which fits well with the contour shape and reduces idle times. However, insufficient continuity between offset curves and limited radial tool engagement over portions of the path often leads to load fluctuations [14]. While adaptive feed rate control partially compensates for these deviations, it does not fully resolve tool load instability [15].

Although contour-parallel strategies generally outperform direction-parallel ones, neither can guarantee constant tool load and smooth path geometry. These shortcomings have driven research and development toward continuous curvature tool paths. Two fundamental approaches exist for generating such trajectories. One involves post-processing classic tool paths to smooth sharp direction changes and achieve the desired continuity [16–18]. The other directly generates tool paths with appropriate continuity [19, 20]. The latter approach characterises modern strategies where tool load dynamics and path curvature are integral design parameters. Within this framework, spiral and trochoidal strategies are most commonly applied for rough machining.

Spiral tool paths are highly advantageous in HSM due to their lack of corners and sharp direction changes, making them popular for both freeform surface finishing and rough pocket milling [21]. The simplest spiral tool paths are typically derived by modifying contour-parallel strategies through overlapping offset curves to produce a spiral trajectory [22]. Although this improves path continuity, dealing with non-monotonic areas remains difficult, and fundamental limitations of contour-parallel approaches remain [23, 24]. Conversely, truly advanced spiral tool paths are initially designed to ensure curvature continuity [25], thereby satisfying HSM requirements [26–29] – even for components that require multi-axis machining [30].

Trochoidal tool paths facilitate both continuous curvature and controlled tool engagement [31], making them ideal for machining narrow regions such as grooves, corners, or elongated geometries [32, 33]. Certain implementations also optimise path length alongside engagement control, significantly reducing cycle time [34, 35].

These modern algorithms, however, operate efficiently only for specific geometries. Trochoidal strategies are rarely used alone for complete pocket machining but are primarily applied in hard-to-reach or critical zones [36]. Spiral strategies, in contrast, are beneficial mainly in

easily accessible pocket areas. Consequently, maximal efficiency for complex geometries is achieved by combining multiple strategies into so-called hybrid approaches. Zhai et al. [20] and Huang et al. [37] integrated spiral and contour-parallel paths, applying HSM-appropriate spiral trajectories in the pocket centre and reduced feed contour paths at the edges. Dumitrache and Borangiu [38] developed a combined method that ensures constant engagement and smooth machining with spiral paths centrally and trochoidal features along the edges.

1.3 Advanced CAM strategies

CAM developers have also pursued roughing tool paths, ensuring more uniform tool load distribution. Recognising the potential of hybrid path generation, CAM solutions increasingly reflect this direction [38–40]. Various developers introduced different implementations, all fundamentally aiming to maintain consistent tool engagement [41–44].

TrueMill (2005) was one of the earliest solutions to implement a variable stepover to ensure a constant engagement angle, while keeping feed rate, spindle speed, and axial depth of cut fixed. Notably, trochoidal segments were applied not only at corners but also within the central regions of pockets [45, 46]. Later, VoluMill (2008) introduced a strategy focused on maintaining a constant material removal rate by varying the engagement angle and adapting the feed accordingly. It primarily follows contour-parallel paths, enhanced with trochoidal motions in high-load regions [47]. Similarly, Adaptive Milling (2011) emphasised maintaining a consistent engagement angle throughout the tool path to ensure uniform tool loading [48].

Other systems developed in subsequent years have built upon these foundations. Although their implementations vary, they generally integrate smooth spiral or contour-parallel paths with adaptive feed rate control and strategically placed trochoidal segments to reduce tool wear and improve machining efficiency. Some solutions – such as *iMachining* – go even further by accounting for machine tool dynamics and acceleration limits, thereby enhancing overall tool path stability and performance. [49]

1.4 Lamé curves

Lamé curves and their generalisations – superellipses and superellipsoids (refer to Fig. 1) – play a significant role in various fields of mathematical modelling, mechanical engineering, and applied mechanics. Initially introduced by Gabriel Lamé in 1818, these curves describe smooth, convex shapes governed by a power-type equation. Over the centuries, researchers have expanded and adapted

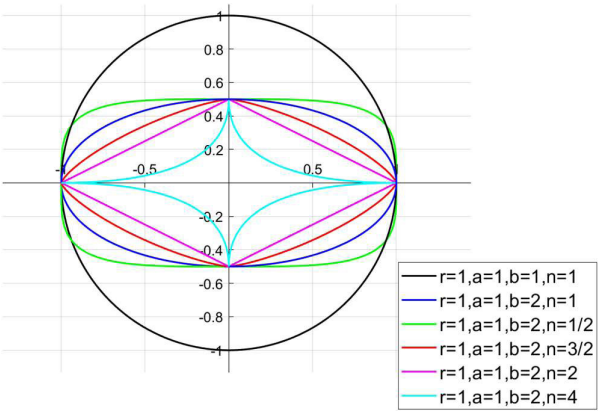

Fig. 1 The shape of Lamé curves with varying parameters

the concept to model increasingly complex and realistic geometries across scientific and engineering domains.

One of the most impactful directions in recent research is the generalisation of superellipsoids by introducing distinct power exponents for each coordinate direction. This refinement, developed by Ni et al. [50], allows for more flexible and accurate modelling of real-world components with anisotropic or non-uniform geometry. In structural mechanics, Altekin and Altay [51] analysed point-supported superelliptical plates under uniform loading, addressing a gap in the literature despite the common industrial use of such geometries. In biomechanics, superellipsoids have been used by Bayraktar et al. [52] and Rincón-Kohli and Zysset [53] to formulate accurate yield criteria for trabecular bone, enabling realistic simulation of biological materials under physiological stress. Lamé curves have also been applied in extended target tracking problems with contour-based measurements [54] and in UAV path planning, where their smooth curvature properties enable efficient and feasible trajectory design around constrained environments [55]. They have also been used in vision-based measurement systems for estimating body and clothing circumferences, where Lamé curves outperformed traditional elliptical approximations [56].

Beyond technical domains, the superellipse has also left a mark on design and aesthetics. Danish mathematician, designer, and poet Piet Hein rediscovered the superellipse independently in the 20th century and popularised its use in architecture, urban planning, and industrial design. His most well-known project is the Sergels Torg roundabout in Stockholm, designed as a superellipse.

Despite their versatility and proven utility in mechanics, biomechanics, and design, superellipses and superellipsoids have not yet been applied to tool path generation, where geometric flexibility and load uniformity are equally critical. This work is the first to explore their potential in this context, apart from our previous brief contribution [57].

This paper introduces a novel spiral tool path that efficiently meets modern HSM requirements for simple geometries. Existing direction-parallel or contour-parallel methods involve sharp corners, negatively affecting cutting conditions. Although hybrid solutions offer smoother paths, they contain unproductive looping segments that increase cycle time. Prior research on spiral paths has primarily been limited to circular spirals and has not explored the application of Lamé curves to achieve continuous spiral transitions between differing shapes. This study presents an innovative Lamé curve-based spiral tool path generation method that enables continuous transitions between polygonal geometries, enhancing tool load uniformity and reducing cycle times. This is achieved via a simple polar equation, resulting in a highly continuous path with minimal computational demand.

In this paper, Section 1 reviews the field, outlines the limitations of traditional strategies, highlights modern technologies, and presents examples of advanced solutions implemented in CAM systems. Section 2 presents the steps of tool path generation, from defining the geometry to adjusting path-related parameters. Section 3 describes the experimental setup, the geometries used, the results obtained, and their evaluation. The conclusions are summarised in Section 4.

2 Tool path generation using Lamé curves

2.1 Mathematical background

The Lamé curve was described first by Gabriel Lamé, a French mathematician and physicist, in the 19th century in the following form:

$$r = \left(\frac{x}{a}\right)^n + \left(\frac{y}{b}\right)^n \tag{1}$$

The Lame curve can be described in implicit form Eq. (2), and in parametric form Eq. (3):

$$r = \left|\frac{x}{a}\right|^n + \left|\frac{y}{b}\right|^n \tag{2}$$

$$x(t) = \frac{r\cos(t)^n}{a}, \quad y(t) = \frac{r\sin(t)^n}{b} \tag{3}$$

The a parameter belongs to the major, b belongs to the minor axis. The r parameter is the scale factor, and the exponent is n.

The exponent results in a different curve depending on the equation type (implicit or parametric). Table 1 summarises the various cases. Using the implicit form is slightly difficult because its application range is limited, and two segments are necessary to create a complete closed curve. The parametric form is more suitable for generating a closed curve, and therefore, it is used for further deduction. In Fig.1, more samples are represented, using the parametric form and different parameter combinations. It can be seen that the exponent n controls the shape from a diamond through an ellipse to a rectangle. If the desired contour is a rectangle, the exponent can effectively control the corner radius.

Table 1 The shape of the Lamé curve with different n exponent

	$n < 1$	$n = 1$	$1 < n < 2$	$n = 2$	$2 < n$
Implicit	concave	linear	convex	convex	convex
Parametric	convex	convex	convex	linear	concave

It is a convenient form for closed curves or spirals using polar functions in a polar coordinate system. Furthermore, it allows for easy transformations; therefore, it is applied. The polar radius can be expressed with the two parametric equations (Eq. (3)) using the general expression: $r = \sqrt{(x)^2 + (y)^2}$ and results in Eq. (4). The order of power is important to avoid discontinuity. First has to be the square, after the n power.

$$r_{polar} = \sqrt{\left(\frac{r}{a}\right)^2 \left(\cos(t)^2\right)^n + \left(\frac{r}{b}\right)^2 \left(\sin(t)^2\right)^n} \tag{4}$$

The next step is to express the polar angle, φ. The tangent of the polar angle can be expressed with the component equation (Eq. (3)) in Eq. (5):

$$\tan(\varphi) = \frac{\sin(t)^n a}{b\cos(t)^n} \tag{5}$$

The Eq. (5) can be solved for φ in Eq. (6):

$$\varphi = \arctan\left(\frac{\tan(t)^n a}{b}\right) \tag{6}$$

While the polar equation can contain only φ, the t parameter has to be expressed with this in Eq. (7):

$$t(\varphi) = \arctan\left(\left(\frac{\tan(\varphi) b}{a}\right)^{\frac{1}{n}}\right) \tag{7}$$

Substituting Eq. (7) into Eq. (8), after simplification and reordering, the result is the polar equation of the Lamé curve, Eq. (8):

$$r_{polar}(\varphi) = \frac{r}{a}\left(1 + \left(\frac{\tan(\varphi)^2 b^2}{a^2}\right)^{\frac{1}{n}}\right)\sqrt{1 + \tan(\varphi)^2} \tag{8}$$

For pocket milling, generally, spiral curves are used (refer to Fig. 2). The Lamé curve can be transformed to satisfy this requirement. First, the radial pitch per revolution has to be defined in Eq. (9):

$$p = \frac{P}{2\pi} \tag{9}$$

For a given rectangle, its envelope curve has a different side ratio than the original.

Thus, the a and b factors can not be constant, a new α and β factor must be defined. The r/α and r/β ratio in the function of φ is described in Eq. (10).

$$\begin{aligned} \frac{r}{\alpha} &= p \quad \varphi + \frac{r}{a} \\ \frac{r}{\beta} &= p \quad \varphi + \frac{r}{b} \end{aligned} \tag{10}$$

From Eq. (10), the desired α and β factors can be expressed in Eq. (11):

$$\begin{aligned} \alpha &= \frac{r\,a}{r + p\,\varphi\,a} \\ \beta &= \frac{r\,b}{r + p\,\varphi\,b} \end{aligned} \tag{11}$$

After substitution, the final equation of a Lame spiral can be revealed in Eq. (12):

$$r_{polar}(\varphi) = \frac{r + p\,\varphi\,a}{a} \left(1 + \left(\frac{\tan(\varphi)^2\, b^2\, (r + p\,\varphi\,a)^2}{(r + p\,\varphi\,b)^2\, a^2} \right)^{\frac{1}{n}} \right)^{-\frac{n}{2}} \sqrt{1 + \tan(\varphi)^2} \tag{12}$$

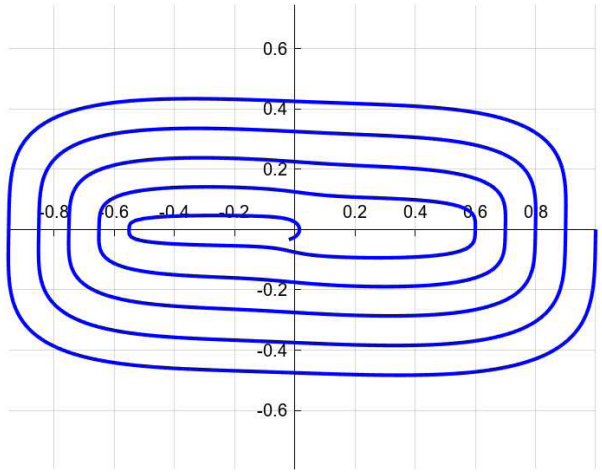

Fig. 2 Sample geometry of Lamé spiral, the parameters are: $r = 1$, $a = 1$, $b = 2$, $n = 1/2$, $p = 0.1/(2\pi)$

Using $\varphi = C1\varphi + C0$ substitution, the spiral can be rotated with $C0$, and a polygon shape can be obtained. If the sides of the polygon are m, then $C1 = m/4$.

These curves can be used for pocket milling in the case of symmetrical and simple geometry. It must be noted that the a, b, n and m can be not only constant, but also a function of φ. The parameters a and b define the scaling of the spiral along the x and y axes, respectively, while m controls the number of corners, allowing smooth transitions between different shapes. The most important parameter is n, which controls the shape, the curvature and cutter engagement; lower n values result in more angular shapes (see Table 1). Another key parameter is p, which governs the radial step size of the spiral and thereby affects both the stepover and the cutter engagement.

The derivative function of Eq. (12) exists and allows for drawing the inner and outer envelope curves. The envelope curves are necessary to calculate the cutter engagement.

2.2 Application for open and closed machining areas

The mathematical formulas outlined previously can be used to generate tool paths for both pocket-like (closed) and island-like (open) geometries. In the case of pockets, machining is performed from the inside out. The boundary of the helical immersion at the centre of the pocket serves as one reference curve, while the pocket wall represents the other reference curve, which must be continuously connected by a Lamé spiral. For island geometries, machining is conducted from the outside in. When defining the spiral curve for islands, an intermediate elliptical shape is also required, from which the Lamé spiral can continuously trace both the contour of the island and the stock boundary. Practical examples of implementations are described in Section 3.3.

2.3. Feed rate adjustment

Once the tool path was calculated, a self-developed algorithm [58] was used to determine the cutter engagement angle along the path. Using the calculated cutter engagement angle, the following formula can be applied to adjust the feed rate to ensure a uniform material removal rate:

$$v_{f,adj}(\theta) = v_{f,nom} \frac{1 - \cos(\theta_{nom})}{1 - \cos(\theta)} \left[\frac{\text{mm}}{\text{min}} \right] \tag{13}$$

where θ [°] is the calculated cutter engagement at a given point, θ_{nom} is the nominal cutter engagement, and $v_{f,nom}$[mm/min] is the feed rate for the nominal cutter engagement.

The tool path was divided into segments using 0.5 mm long linear sections. Then the NC program was generated using the smaller feed value calculated at both endpoints of the segments. Thanks to the continuous curvature and the gradual changes in cutter engagement along the Lamé spiral, the feed rate adjustment can be applied smoothly and remains dynamically stable, avoiding critical acceleration demands or vibration issues.

3 Experimental validation

Cutting and simulation experiments were conducted to evaluate the developed Lamé curve-based tool path generation strategy. The experimental conditions are detailed in Section 3.1, and the machining features investigated are described in Section 3.2. Two commonly used tool path planning methods, contour-parallel and adaptive milling strategies, were utilized as references to evaluate the developed algorithm. These tool paths were generated using the NX CAM software (version: NX 2000). The investigated tool paths are presented in Section 3.3. The results of the simulation, including the tool path length and cutter engagement, are presented in Section 3.4. The force measurement results from the cutting experiments are provided in Section 3.5.

3.1 Experimental environment

The experimental setup is shown in Fig. 3. The cutting experiments were performed on a Kondia B640-type 3-axis machining centre, where Al6082 aluminium alloy was machined with a four-edged solid carbide flat end mill coated with Alcrone. The end mill had a helix angle of 30° and a diameter of ∅6 mm (Tivoly, No. 82365610600). The cutting speed (v_c) was set at 150 m/mm, considering the limitations of the machine tool spindle, while the feed per tooth (f_z) was 0.04 mm, as recommended by the cutting tool's catalogue. This resulted in a programmed spindle speed (n) of 7962 rpm and a feed rate (v_f) of 1274 mm/min. Since the purpose of the experiments was a comparative analysis, the axial depth of cut (a_p) was reduced to 2 mm, while the nominal radial depth of cut (a_e) was set at 25% of the tool diameter. To improve the uniformity and direction independence of the flood coolant, a Loc-Line circle flow nozzle kit was used.

During the cutting experiments, in addition to recording the cycle time, the cutting force was measured using a Kistler 9257B piezoelectric dynamometer. During signal processing, a low-pass filter was applied to suppress external noise. The cut-off frequency was set to ten times the spindle speed, and the magnitude of the calculated force projected onto the machining plane (X-Y) was analyzed to assess the tool load. To enhance clarity, the maximum values per tool revolution will be displayed on the force measurement diagrams.

3.2 Sample geometries

Four sample geometries were selected to test the developed path planning strategy based on Lamé curves, comparing it with currently available methods. The roughing of the closed areas was performed using two pockets, with the outer contour being either a square or a hexagon inscribed in a ∅25 mm diameter circle. For the open areas, we tested the roughing strategy by machining two island geometries, each featuring a square and a hexagon inscribed in a ∅15 mm diameter circle, positioned in the middle of a workpiece with a enclosure size. The geometric designs can be found in the figures depicting the tool paths in Section 3.3.

3.3 Tool path generation

As mentioned above, three tool path generation strategies were examined: the contour-parallel milling (Fig. 4), the adaptive milling (Fig. 5), and the developed Lamé curve-based tool path (Fig. 6).

Fig. 3 The experimental setup for cutting tests and a machined hexagonal island shaped by a Lamé curve

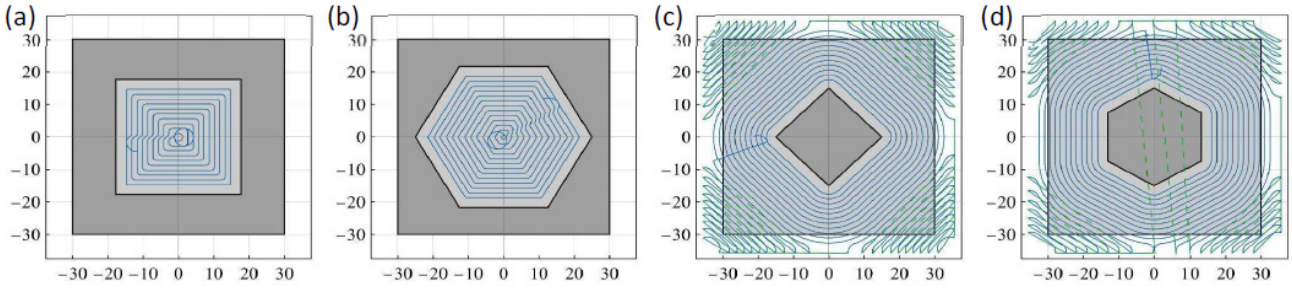

Fig. 4 The contour-parallel tool paths: (a) squared shape pocket; (b) hexagon-shaped pocket; (c) square-shaped island; (d) hexagon-shaped island

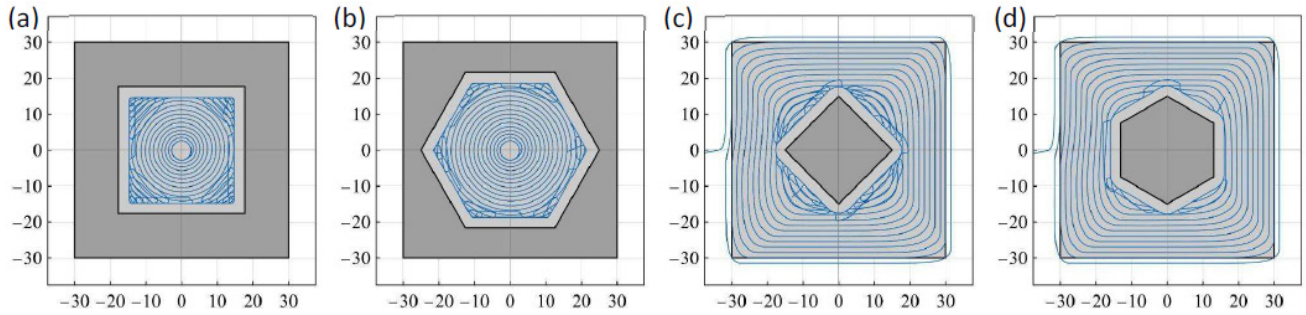

Fig. 5 The adaptive milling. tool paths: (a) squared shape pocket; (b) hexagon-shaped pocket; (c) square-shaped island; (d) hexagon-shaped island

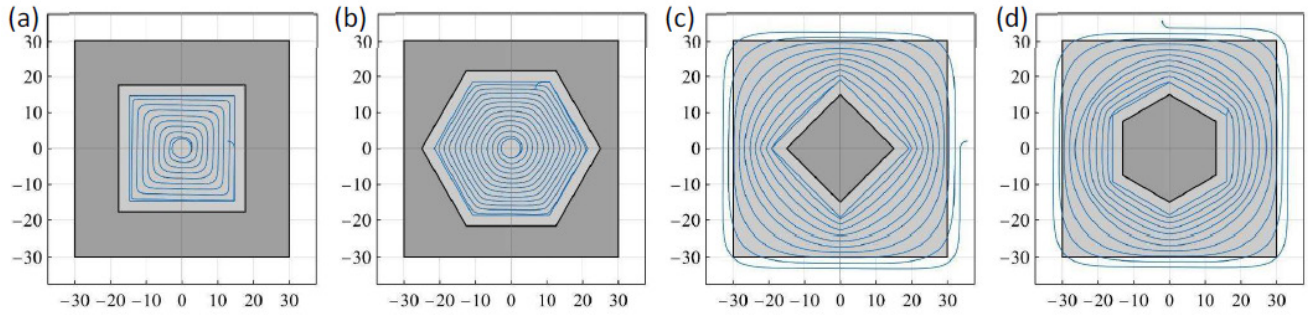

Fig. 6 The Lamé curve-based tool paths: (a) squared shape pocket; (b) hexagon-shaped pocket; (c) square-shaped island; (d) hexagon-shaped island

A well-known shortcoming of the contour-parallel strategy is the presence of sharp corners along the tool path, which decrease the feed rate and significantly increase the cutter engagement locally. To address this problem, the corner smoothing function in the NX CAM software was used, and 1 mm rounding radii were applied to the path at each corner. Additionally, an MRR-based automatic feed control function is available in NX CAM that applies adaptive feed rates to the tool path. However, the built-in algorithm generates the NC program with longer segments than an own-developed algorithm, so the feed rate scheduling algorithm used for Lamé curve-based paths was also utilised for contour-parallel paths.

The NX CAM's Adaptive milling cycle meets the requirements of high-speed machining by providing a smooth tool path and uniform tool load. However, this comes at the cost of looped sections during trochoidal-like machining. The presence of these unproductive linking motions provides an opportunity for other tool path planning strategies to achieve shorter cycle times.

For the chosen sample geometries, the following mathematical considerations were taken into account for tool path generation. In all cases, r, a, b and p were constant The φ parameter was simply multiplied by a constant, as the polygonal shape requires. The n exponent was the linear function of φ, which provides a linear transition between v_1 and v_2, while φ changes between τ_1 and τ_2. Using this, the curvature of the tool path can be smoothly fitted to the corners while the path is getting closer to the final contour.

In case of the squared shape pocket (Fig. 6 (a)), the substituted constant parameters are the following: $r = 14.7$, $a = 1$, $b = 1$, $\varphi = 0 + 4/4\ \varphi$, $p = 1.5/(2\pi)$. The exponent is a linear function of φ:

$$n = \frac{(v_2 - v_1)}{(\tau_2 - \tau_1)\cdot(\varphi - \tau_1) + v_1} \tag{14}$$

where $\tau_1 = -61.583$ and $\tau_2 = 0$ are the start and endpoint, $v_1 = 0.9$ and $v_2 = 0.1$ are the values of the exponent at the start and endpoint.

In case of the hexagon-shaped pocket (Fig. 6 (b)), the substituted constant parameters are the following: $r = 21.0$, $a = 1$, $b = 1$, $\varphi = 0 + 6/4\ \varphi$, $p = 4/6 \cdot 1.5/(2\pi)$ The exponent is a linear function of : see Eq. (14), where $\tau_1 = -88.0$ and $\tau_2 = 0$ are the start and endpoint, $v_1 = 0.9$ and $v_2 = 1.36$ are the values of the exponent at the start and endpoint.

For the manufacturing of islands, two Lamé curves were combined, which gave a sufficient tool path. The manufacturing differs from pocket milling because the tool moves from outside to inside. It has to be noticed that the polar angle is decreasing while the tool moves; thus, reverse tracking of the polar angle is achieved. By the first Lamé spiral, the value of the exponent is changed, following the shape of the workpiece, and then becomes similar to a circle. By the second Lamé spiral, the value of the exponent is changed, which joins to the previous circular shape and then follows the contour of the island.

In case of the square-shaped island (Fig. 6 (c)), the substituted constant parameters in the first Lamé spiral are the following: $r = 35.0$, $a = 1$, $b = 1$, $\varphi = 0 + 4/4\ \varphi$, $p = 4/4 \cdot 1.5/(2\pi)$. The exponent is a linear function of φ: see Eq. (14), where $\tau_1 = -16/3 \cdot (2\pi)$ and $\tau_2 = 0$ are the end and startpoint, $v_1 = 0.99$ and $v_2 = 0.01$ are the values of the exponent at the end and startpoint.

The substituted constant parameters in the second Lamé spiral are the following: $r = 18.5$, $a = 1$, $b = 1$, $\varphi = 0 + 4/4\ \varphi$, $p = 4/4 \cdot 1.5/(2\pi)$. The exponent is a linear function of φ: see Eq. (14), where $\tau_1 = -5/2 \cdot (2\pi)$ and $\tau_2 = 0$ are the end and startpoint, $v_1 = 1.01$ and $v_2 = 1.9$ are the values of the exponent at the end and startpoint.

In case of the hexagon-shaped island (Fig. 6 (d)), the substituted constant parameters in the first Lamé spiral are the following: $r = 35.0$, $a = 1$, $b = 1$, $\varphi = 0 + 4/4\ \varphi$, $p = 4/4 \cdot 1.5/(2\pi)$. The exponent is a linear function of φ: see Eq. (14), where $\tau_1 = -16/3 \cdot (2\pi)$ and $\tau_2 = 0$ are the end and startpoint, $v_1 = 0.99$ and $v_2 = 0.01$ are the values of the exponent at the end and startpoint.

The substituted constant parameters in the second Lamé spiral are the following: $r = 18.5$, $a = 1$, $b = 1$, $\varphi = 0 + 6/4\ \varphi$, $p = 4/6 \cdot 1.5/(2\pi)$. The exponent is a linear function of φ: see Eq. (14), where $\tau_1 = -5/2 \cdot (2\pi)$ and $\tau_2 = 0$ are the end and startpoint, $v_1 = 1.05$ and $v_2 = 1.3$ are the values of the exponent at the end and startpoint.

3.4 Simulation analysis

The tool paths described above underwent simulation tests, during which the path length and the evolution of cutter engagement were analysed. The distributions of cutter engagement values calculated with steps of 0.2 mm along the path are represented in the histograms shown in Fig. 7.

In the case of the contour-parallel strategy, it can be seen that the 60° cutter engagement angle corresponding to a 25% stepover was only valid for less than half of the path. When transitioning between offset curves, there is no cutting along the linking movements, which is indicated by a cutter engagement angle of 0°. This non-productive part of the tool path can even become predominant in island-like geometries, where the path length (L) has significantly increased. However, in other areas of the tool path, the cutter engagement angle significantly exceeded the nominal value during pocket milling.

The diagrams indicate that the adaptive milling strategy maintains a well-controlled tool load along the path, the cutter engagement angle consistently staying below the set maximum of 60°. However, this requires the use of looped path sections in certain areas. For the geometries tested, these unproductive sections represented 5–25% of the total path length, which results in increased cycle time.

In the case of the Lamé curve-based tool path, the cutter engagement slightly deviates from the nominal value due to the characteristics of the path. However, this value does not drop to zero, as no linking sections are involved. Furthermore, the maximum cutter engagement angle during pocket machining is lower than that in the contour-parallel machining, because the cutter engagement fluctuates within a narrower range. Since there are no erratic changes thanks to the continuous curvature of the path, the feed rate scheduling algorithm can more effectively compensate for these fluctuations, ensuring a uniform tool load.

3.5 Cutting experiments

3.5.1 Preparatory experiment for testing the MMR-based feed rate scheduling

As mentioned earlier, an MRR-based feed rate scheduling method was employed to address the varying cutter engagement in both the contour parallel and Lamé curve-based strategies. However, due to the complex relationship between cutting parameters and cutting force, this approach only provides a geometric solution for standardising the tool load control. Before comparing the tool path planning strategies, simple side milling experiments were also conducted with different stepovers from 0.75 mm to 6 mm to assess the effectiveness of the MRR-based feed rate adjustment.

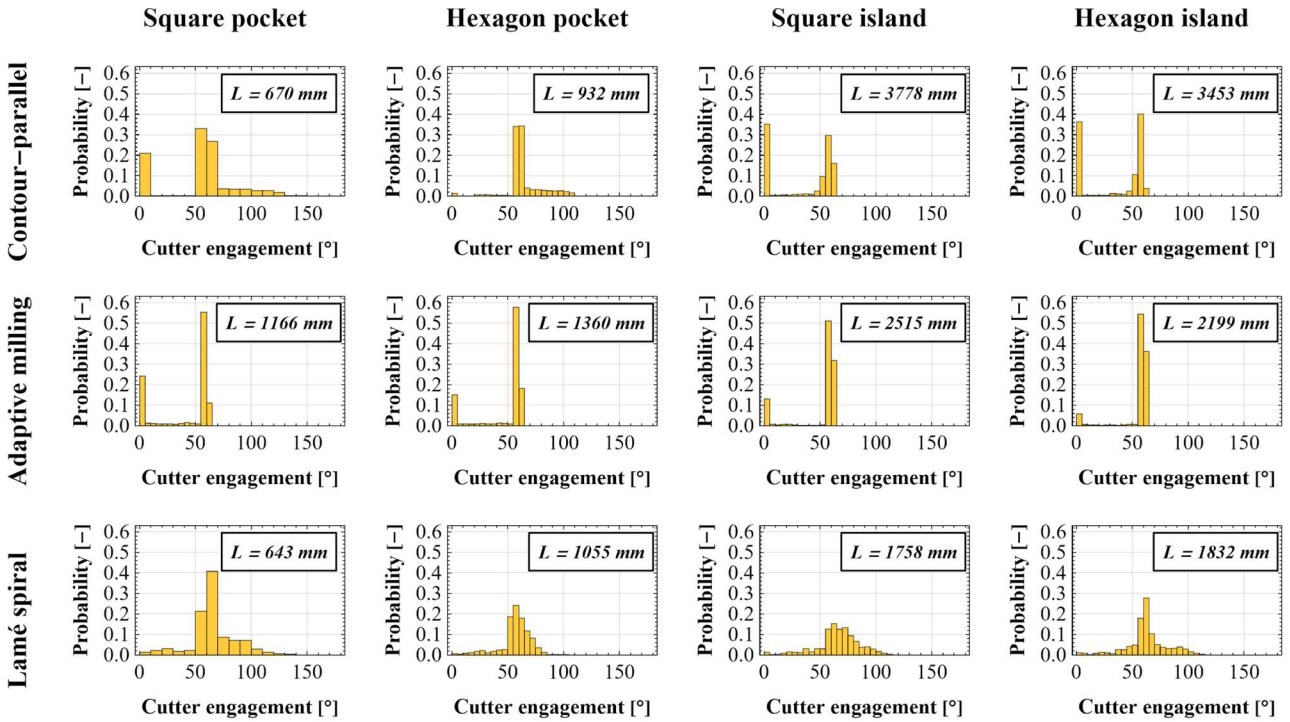

Fig. 7 The cutter engagement distributions and tool path lengths

The results of the preliminary experiment (Fig. 8) indicated that when the stepover was below the nominal value, the cutting force remained close to the value of 238 N measured at the nominal stepover. Therefore, the feed rate increase based on the MRR was appropriate. Although a slight increase in the measured force was observed when the stepover was between 25% and 50% of the tool diameter, it remained within acceptable limits (the relative increase was between 5–10%). For stepovers greater than 50%, the reduction in feed rate, driven by constant MRR, led to lower cutting forces (the relative decrease was between 10–20%). This occurs because when the cutter engagement exceeds 90°, the maximum chip thickness consistently equals the feed

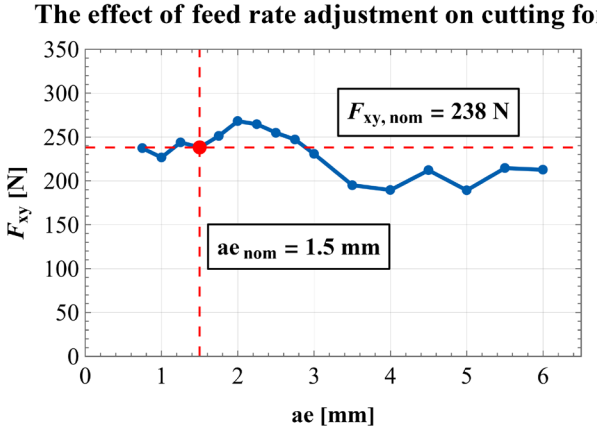

Fig. 8 The Lamé curve-based tool paths

per tooth. However, since the force is distributed over a larger area of the helical-shaped tool edge, a lower resultant cutting force is necessary to keep the cutting torque under control.

In summary, it can be concluded that the MRR-based feed rate adjustment operated reliably in the machining environment used for the experiments.

During the machining of the sample geometries, the measured forces indicated that the tool had to endure significantly higher loads than the nominal force recorded during linear contour milling with nominal parameters. In addition to the fluctuation of the cutter engagement, the explanation for this is that the side wall of the workpiece blocked the coolant from reaching the tool differently at various points along the path. This issue was observed even with the adaptive milling strategy, where the cutter engagement was kept within strict limits, yet the maximum measured force values still exceeded the expected nominal value by 20–40%. Nonetheless, the experiments are fully comparable, as the obstructions affected all strategies similarly.

3.5.2 Machining of pocket geometries

Figs. 9 and 10 show the cutting forces measured during the milling of square and hexagon-shaped pocket geometries, respectively. A problem caused by the partially blocked flood coolant discussed earlier is especially critical for pocket milling paths, as the shape of the allowance is difficult to access. Accordingly, the maximum force values were 359 N

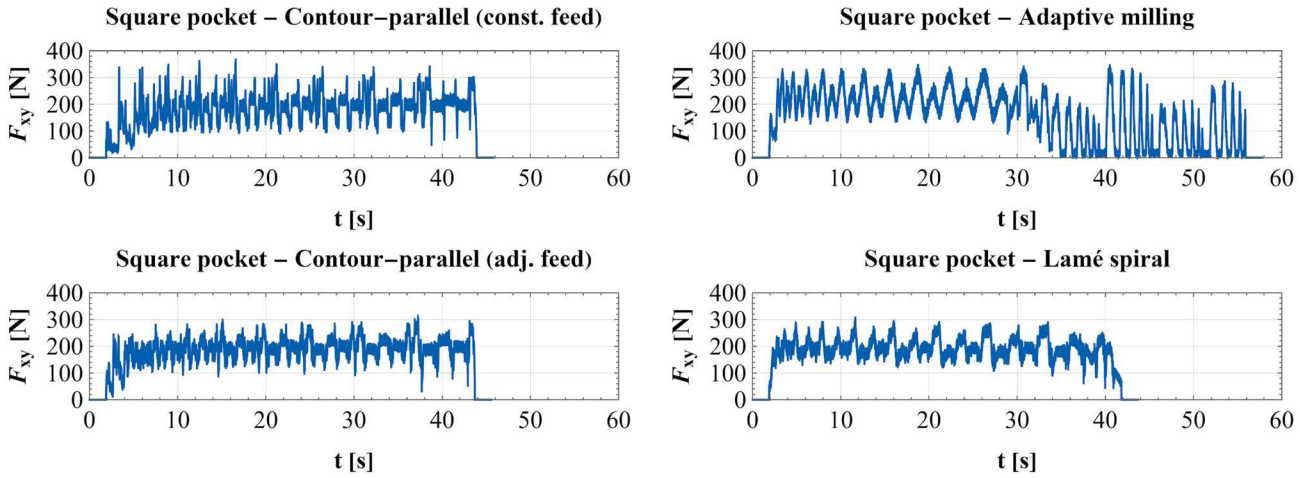

Fig. 9 The measured cutting forces when machining the square-shaped pocket geometry

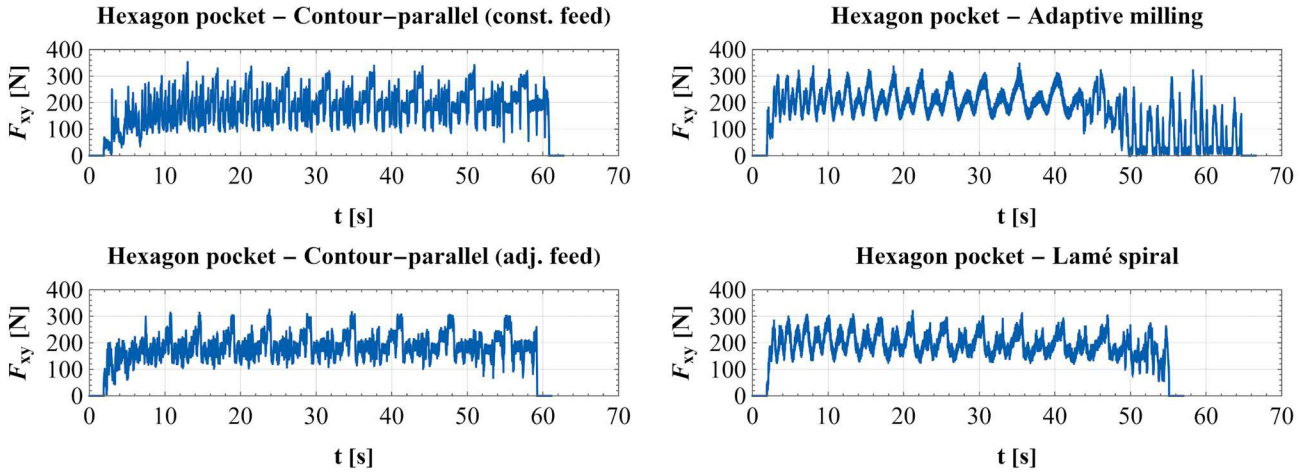

Fig. 10 The measured cutting forces when machining the hexagon-shaped pocket geometry

and 343 N for the contour-parallel tool path with constant feed, 359 N and 343 N with adjusted feed, and 338 N for both geometries with the adaptive milling strategy. However, the Lamé curve-based tool path exhibited the lowest tool load for both geometries, 298 N and 311 N, respectively.

In addition to having the lowest tool load, the Lamé curve-based tool path also demonstrated the shortest machining times, namely 40 s and 54 s. This is compared to 43 s and 60 s for the contour-parallel strategy with constant feed, 43 s and 58 s for the contour-parallel strategy with adjusted feed, and 55 s and 64 s for the adaptive milling strategy. In other words, the advantages of the spiral-like strategy were evident in the pocket milling paths, as the developed Lamé curve-based strategy proved to be the most favourable for the sample geometries examined, both in terms of machining time and tool load.

3.5.3 Machining of island geometries

Some fluctuations in cutting force were also observed for the island geometries across all strategies, but the peak values were lower due to the less enclosed allowance shape. The maximum force values recorded (Figs. 11 and 12) were as follows: 304 N and 291 N for the contour-parallel tool path with a constant feed, 277 N and 255 N contour-parallel tool path with the adjusted feed, and 304 N and 294 N for the adaptive milling strategy. In contrast, the Lamé curve-based tool path showed low tool load for both geometries, measuring 267 N. Therefore, in terms of cutting forces, only the contour-parallel strategy with adaptive feed matched the performance of the developed Lamé spiral strategy, while all other strategies exhibited higher tool loads.

However, regarding machining time, the contour-parallel strategy performed poorly for the geometries examined. Since the allowance shape was broken into several parts, numerous linking movements were needed in the path, leading to longer machining times. Specifically, the machining times were 192 s and 168 s for the contour-parallel strategy with constant feed, and 177 s and 156 s for the contour-parallel strategy with adjusted feed. In contrast, the adaptive milling strategy achieved machining times

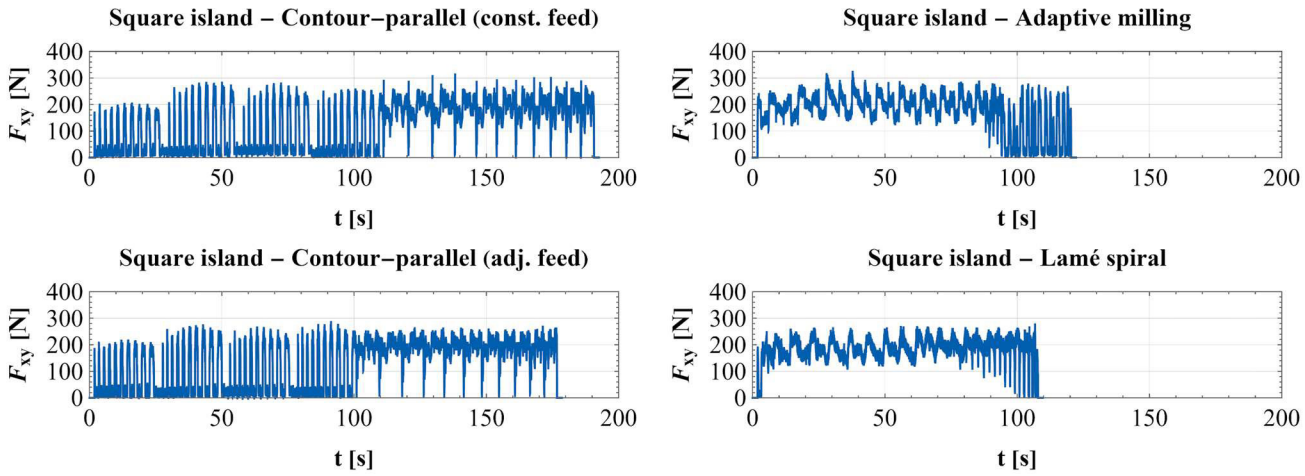

Fig. 11 The measured cutting forces when machining the square-shaped island geometry

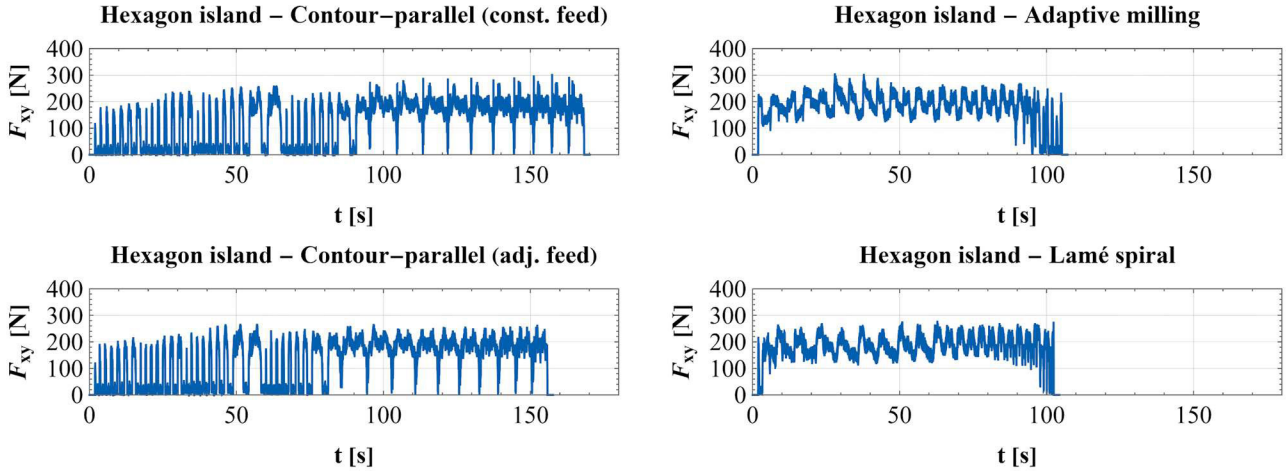

Fig. 12 The measured cutting forces when machining the hexagon-shaped island geometry

of only 120 s and 105 s, while the Lamé curve-based strategy recorded times of 108 s and 103 s. Thus, from a cycle time perspective, the developed strategy significantly outperformed the contour-parallel strategy and even slightly surpassed the adaptive milling strategy. Therefore, when considering both tool load and machining times, the Lamé curve-based strategy was also the most favourable option for the island geometries examined.

3.6 Conclusions and future work

Although the measurement results for each geometry and machining strategy have been presented above, these data have also been summarised in bar charts for enhanced clarity (Fig. 13).

In the contour-parallel strategy, feed rate adjustment improves both machining time and tool load control. Adjusting the feed rate prevents overloads in areas with a large cutter engagement by reducing the feed, while it saves time in segments with a small cutter engagement by increasing the feed. When dealing with pocket-like geometries, where the tool path leads along concave corners, adjusting the feed rate significantly reduces force. In contrast, for island-like geometries, increasing the feed rate helps save time at convex arcs.

In the case of island-like geometries, the adaptive milling strategy resulted in significantly shorter machining times compared to contour-parallel paths, mainly due to fewer linking movements. However, the adaptive milling strategy also included trochoidal sections in the pocket milling paths, which led to slightly longer machining times. Therefore, while the tool load control with the adaptive milling strategy is effective, there is still room for improvement regarding the cycle time.

On the contrary, it has to be noticed that the proposed Lamé curve-based strategy can generate the tool path with a single continuous spiral, eliminating the need for linking

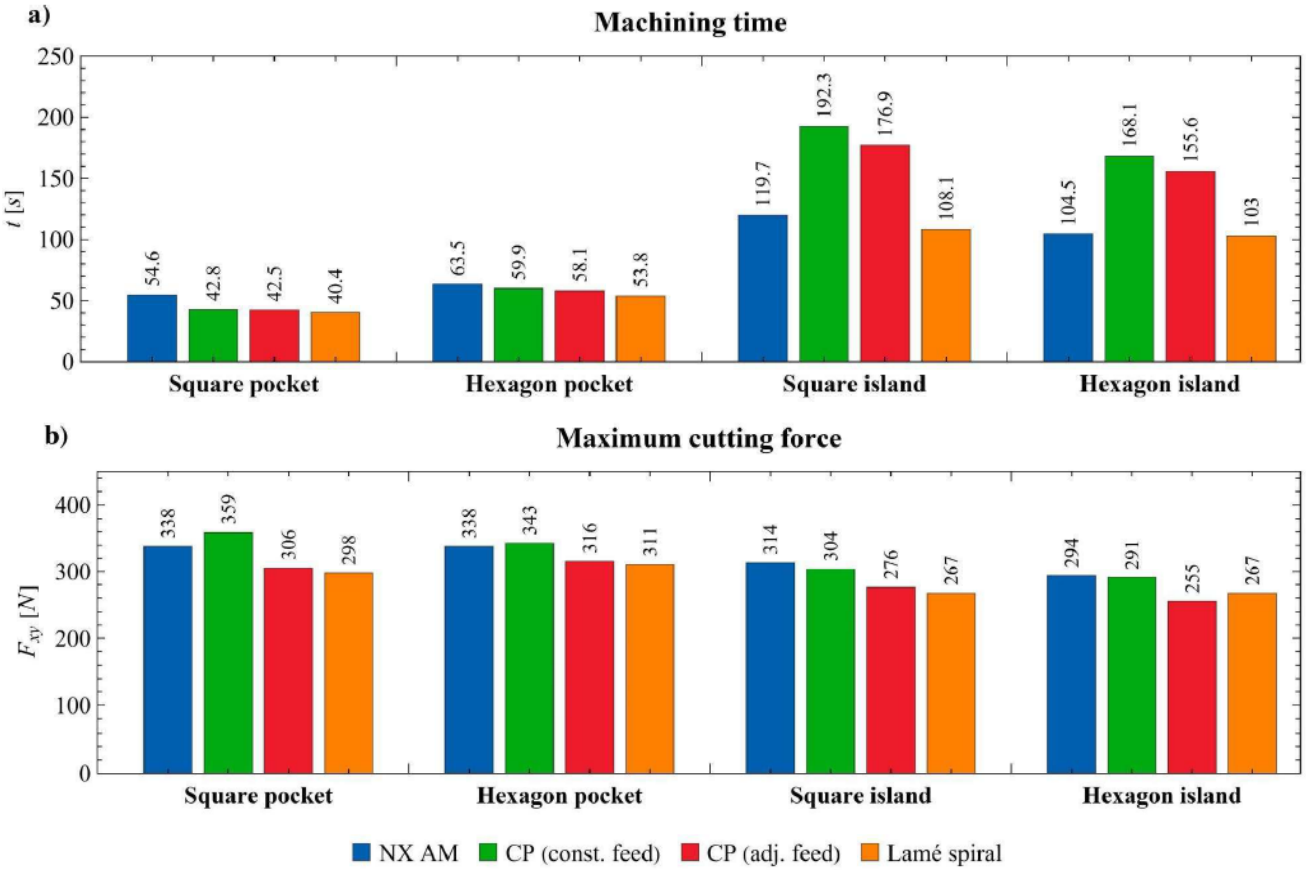

Fig. 13 The comparison of the measured (a) machining times and (b) cutting forces

movements in both pocket and island geometries. While this approach may lead to some fluctuations in the cutter engagement, controlling the feed rate can mitigate its impact on the cutting force. As a result, this solution has shown favourable performance regarding the measured tool load. Although surface roughness was not measured due to the focus on rough milling, the proposed method is not expected to perform worse than the alternative strategies. In fact, the smaller variation in cutter engagement angle and the continuous cutting process could even lead to improved surface quality. In future research, we aim to extend the method to handle more general geometries, including irregular boundaries and pockets with multiple internal features. Moreover, we plan to generalize the approach for multi-dimensional machining tasks and explore its integration as a component within hybrid algorithms. By effectively covering a variety of shapes beyond simple spirals, the Lamé-based approach can nicely complement current hybrid strategies. We also see potential in using AI to optimize parameters like n and p, further improving flexibility and performance.

4 Summary

This paper introduces a newly developed spiral tool path planning strategy that utilises Lamé curves. By appropriately parameterising the Lamé curve, a continuous spiral transition can be achieved between different shapes, thereby allowing for the machining of the allowance material without any linking movements. Although the cutter engagement slightly fluctuates along the path, it remains within a narrow range, allowing for excellent tool load control by adjusting the feed rate. During the algorithm validation, comparisons were made with the traditional contour-parallel strategy and the NX CAM Adaptive milling cycle using four sample geometries: a square-shaped pocket, a hexagon-shaped pocket, a square-shaped island, and a hexagon-shaped island. The following conclusions can be drawn from this analysis:

- by using the Lamé curve-based tool path, there was a 15–25% improvement in machining time for pocket-like geometries and a 1–10% improvement for island-like geometries compared to the adaptive milling strategy; while there was a 5–15% improvement for pocket-like geometries and a 39–44% improvement for island-like geometries compared to the contour-parallel milling strategy
- by using the Lamé curve-based tool path, there was an 8–12% decrease in peak cutting force for pocket-like geometries and a 9–15% improvement for

island-like geometries compared to the adaptive milling strategy; while there was a 3–17% improvement for pocket-like geometries and a 3–12% improvement for island-like geometries compared to the contour-parallel milling strategy (except for the machining of the hexagon-shaped island, where the maximum cutting force was 5% lower for the contour-parallel path with adaptive feed)
- considering the previous results, the developed strategy can be effectively used for roughing operations of both open and closed allowance shapes

Further potential applications include the generation of morphed spiral tool paths for the finishing of free-form surfaces, as well as the creation of tool paths for 3D printing technologies, whether using lasers or filaments. From a practical perspective, the uninterrupted and smooth nature of the tool path offers benefits for industrial applications, such as improved tool life, reduced machine wear, and overall shorter cycle times. Importantly, the reduction in machining time translates directly into cost savings in production, making the proposed strategy not only technically effective but also economically advantageous for industrial use. The proposed method proved to be the most efficient in machining time during the comparative tests, while it is easy to integrate into existing CAM systems, making it readily applicable in many workflows. It is important to note that one of the main limitations of this method is that the two curves, between which a continuous spiral transition must be maintained, need to possess a certain degree of rotational symmetry, in addition to concentricity. There is an opportunity for further development to address these limitations, which would broaden the algorithm's applicability.

Acknowledgment
The project was supported by the Doctoral Excellence Fellowship Programme (DCEP), the University Research Scholarship Programme (EKÖP), the EUREKA project (ID: 2020-1.2.3-EUREKA-2022-00026), the TKP2021-NVA funding scheme (project no. TKP-6-6/PALY-2021) and the project 2021-1.2.4-TÉT-2021-00054 "Machine learning supported process monitoring of micro machining in the frame of Industry 4.0" funded by the National Research Development and Innovation Fund of the Ministry of Culture and Innovation and the Budapest University of Technology and Economics.

References

[1] Hatna, A., Grieve, R. J., Broomhead, P. "Automatic CNC milling of pockets: geometric and technological issues", Computer Integrated Manufacturing Systems, 11(4), pp. 309–330, 1998. https://doi.org/10.1016/S0951-5240(98)00030-5
[2] Held, M. "On the Computational Geometry of Pocket Machining", Springer Berlin, Heidelberg, 1991. ISBN: 978-3-540-47413-5 https://doi.org/10.1007/3-540-54103-9
[3] Póka, G., Mátyási, G., Németh, I. "Burr Minimisation in Face Milling with Optimised Tool Path", Procedia CIRP, 57, pp. 653–657, 2016. https://doi.org/10.1016/j.procir.2016.11.113
[4] Bieterman, M. B., Sandstrom D. R. "A Curvilinear Tool-Path Method for Pocket Machining", Journal of Manufacturing Science and Engineering, 125(4), pp. 709–715, 2003. https://doi.org/10.1115/1.1596579
[5] Siller, H., Rodriguez, C. A., Ahuett, H. "Cycle time prediction in high-speed milling operations for sculptured surface finishing", Journal of Materials Processing Technology, 174(1–3), pp. 355–362, 2006. https://doi.org/10.1016/j.jmatprotec.2006.02.008
[6] Cheng, K. (ed.) "Machining Dynamics: Fundamentals, Applications and Practices", Springer London, 2009. ISBN: 978-1-84628-368-0 https://doi.org/10.1007/978-1-84628-368-0
[7] Jacso, A., Matyasi, G., Szalay, T. "Advanced spiral tool path for circular pocket machining", In: International Conferene on Innovative Technologies (IN-TECH 2015), Dubrovnik, Croatia, 2015, pp. 202–205.
[8] Wang, W. P. "Solid modeling for optimizing metal removal of three-dimensional NC end milling", Journal of Manufacturing Systems, 7(1), pp. 57–65, 1988. https://doi.org/10.1016/0278-6125(88)90033-7
[9] Jacso, A., Szalay, T., Sikarwar, B. S., Phanden, R. K., Singh, R. K., Ramkumar, J. "Investigation of conventional and ANN-based feed rate scheduling methods in trochoidal milling with cutting force and acceleration constraints", The International Journal of Advanced Manufacturing Technology, 127(1), pp. 487–506, 2023. https://doi.org/10.1007/s00170-023-11506-x
[10] Zhou, M., Zheng, G., Chen, Z. C. "An automated CNC programming approach to machining pocket with complex islands and boundaries by using multiple cutters in hybrid tool path patterns", The International Journal of Advanced Manufacturing Technology, 83(1), pp. 407–420, 2016. https://doi.org/10.1007/s00170-015-7506-3
[11] Xu, C.-Y., Li, J.-R., Wang, Q.-H., Hu, G.-H. "Contour parallel tool path planning based on conformal parameterisation utilising mapping stretch factors", International Journal of Production Research, 57(1), pp. 1–15, 2019. https://doi.org/10.1080/00207543.2018.1456699
[12] Held, M. "A geometry-based investigation of the tool path generation for zigzag pocket machining", The Visual Computer, 7(5), pp. 296–308, 1991. https://doi.org/10.1007/BF01905694

[13] Kim, H.-C. "Optimum tool path generation for 2.5D direction-parallel milling with incomplete mesh model", Journal of Mechanical Science and Technology, 24(5), pp. 1019–1027, 2010. https://doi.org/10.1007/s12206-010-0306-7

[14] Hinduja, S., Roaydi, A., Philimis, P., Barrow, G. "Determination of optimum cutter diameter for machining 2.5D pockets", International Journal of Machine Tools and Manufacture, 41(5), pp. 687–702, 2001. https://doi.org/10.1016/S0890-6955(00)00098-5

[15] Bae, S.-H., Ko, K., Kim, B. H., Choi, B. K. "Automatic feedrate adjustment for pocket machining", Computer-Aided Design, 35(5), pp. 495–500, 2003. https://doi.org/10.1016/S0010-4485(01)00195-6

[16] Beudaert, X., Pechard, P.-Y., Tournier, C. "5-Axis tool path smoothing based on drive constraints", International Journal of Machine Tools and Manufacture, 5112, pp. 958–965, 2011. https://doi.org/10.1016/j.ijmachtools.2011.08.014

[17] Yang, J., Hu, Q., Ding, H. "A Two-stage CNC Interpolation Algorithm for Corner Smoothing Trajectories with Geometric Error and Dynamics Constraints", Procedia CIRP, 56, pp. 306–310, 2016. https://doi.org/10.1016/j.procir.2016.10.022

[18] Tajima, S., Sencer, B. "Global tool-path smoothing for CNC machine tools with uninterrupted acceleration", International Journal of Machine Tools and Manufacture, 121, pp. 81–95, 2017. https://doi.org/10.1016/j.ijmachtools.2017.03.002

[19] Xiong, Z.-H., Zhuang, C.-G., Ding, H. "Curvilinear tool path generation for pocket machining", Proceedings of the Institution of Mechanical Engineers, Part B: Journal of Engineering Manufacture, 225(4), pp. 483–495, 2011. https://doi.org/10.1177/2041297510394085

[20] Zhai, Z., Lin, Z., Fu, J. "HSM toolpath generation with capsule-based region subdivision", The International Journal of Advanced Manufacturing Technology, 97(1), pp. 1407–1419, 2018. https://doi.org/10.1007/s00170-018-2035-5

[21] Zhao, H., Gu, F., Huang, Q.-X., Garcia, J., Chen, Y., Tu, C., Benes, B., Zhang, H., Cohen-Or, D., Chen, B. "Connected fermat spirals for layered fabrication", ACM Transactions on Graphics, 35(4), pp. 1–10, 2016. https://doi.org/10.1145/2897824.2925958

[22] Wang, S., Wang, C., Wang, P., Liu, H., Wang, Y. "PDE-based spiral machining trajectory planning method without tool feed marks on 2D arrayed multi-island regions", The International Journal of Advanced Manufacturing Technology, 125(5), pp. 2021–2034, 2023. https://doi.org/10.1007/s00170-022-10702-5

[23] Zhuo, W., Rossignac, J. "Curvature-based offset distance: Implementations and applications", Computers & Graphics, 36(5), pp. 445–454, 2012. https://doi.org/10.1016/j.cag.2012.03.013

[24] Narayanaswami, R., Choi, Y. "NC Machining of Freeform Pockets with Arbitrary Wall Geometry Using a Grid-Based Navigation Approach", The International Journal of Advanced Manufacturing Technology, 18(10), pp. 708–716, 2001. https://doi.org/10.1007/s001700170013

[25] Leroy, C., Lavernhe, S., Rivière-Lorphèvre, É. "Hermite Quartic Splines for Smoothing and Sampling a Roughing Curvilinear Spiral Toolpath", Applied Sciences, 14(17), 7492, 2024. https://doi.org/10.3390/app14177492

[26] Dhanda, M., Kukreja, A., Pande, S. "Adaptive spiral tool path generation for computer numerical control machining using point cloud", Proceedings of the Institution of Mechanical Engineers, Part C: Journal of Mechanical Engineering Science, 235(22), pp. 6240–6256, 2021. https://doi.org/10.1177/0954406221990077

[27] Ge, Z., Hu, Q., Wang, Z., Zhu, Y. "Spiral tool path generation method for complex pocket machining based on electrostatic field theory", Journal of the Brazilian Society of Mechanical Sciences and Engineering, 46(10), 614, 2024. https://doi.org/10.1007/s40430-024-05191-4

[28] Lei, Y., Hou, T., Ding, Y. "Stability analysis of pocket machining with the spiral tool path using the discontinuous Galerkin method", Journal of Manufacturing Processes, 92, pp. 12–31, 2023. https://doi.org/10.1016/j.jmapro.2023.02.028

[29] Szaroleta, M., Treter, G., Nowak, K. "Modified tool radius compensation in the Archimedes' spiral tool path for high speed machining of circular geometry", Journal of Manufacturing Processes, 97, pp. 275–289, 2023. https://doi.org/10.1016/j.jmapro.2023.04.027

[30] Ma, H.-Y., Kou, Y.-B., Shen, L.-Y., Yuan, C.-M. "Efficient tool path planning method of ball-end milling for high quality manufacturing", Robotics and Computer-Integrated Manufacturing, 93, 102905, 2025. https://doi.org/10.1016/j.rcim.2024.102905

[31] Jacso, A., Matyasi, Gy., Szalay, T. "Trochoidal Tool Path Planning Method for Slot Milling with Constant Cutter Engagement", In: Phanden, R. K., Mathiyazhagan, K., Kumar, R., Davim, J. P. (eds.) Advances in Industrial and Production Engineering, Springer Singapore, 2021. pp. 659–668. ISBN 978-981-33-4320-7 https://doi.org/10.1007/978-981-33-4320-7_59

[32] Otkur, M., Lazoglu, I. "Trochoidal milling", International Journal of Machine Tools and Manufacture, 47(9), pp. 1324–1332, 2007. https://doi.org/10.1016/j.ijmachtools.2006.08.002

[33] Rauch, M., Hascoet, J.-Y. "Rough pocket milling with trochoidal and plunging strategies", International Journal of Machining and Machinability of Materials, 2(2), pp. 161–175, 2007. http://doi.org/10.1504/IJMMM.2007.013780

[34] Santhakumar, J., Iqbal, U. M. "Parametric Optimization of Trochoidal Step on Surface Roughness and Dish Angle in End Milling of AISID3 Steel Using Precise Measurements", Materials, 12(8), 1335, 2019. https://doi.org/10.3390/ma12081335

[35] Santhakumar, J., Iqbal, U. M. "Role of trochoidal machining process parameter and chip morphology studies during end milling of AISI D3 steel", Journal of Intelligent Manufacturing, 32(3), pp. 649–665, 2021. https://doi.org/10.1007/s10845-019-01517-5

[36] Elber, G., Cohen, E., Drake, S. "MATHSM: medial axis transform toward high speed machining of pockets", Computer-Aided Design, 37(2), pp. 241–250, 2005. https://doi.org/10.1016/j.cad.2004.05.008

[37] Huang, N., Lynn, R., Kurfess, T. "Aggressive Spiral Toolpaths for Pocket Machining Based on Medial Axis Transformation", Journal of Manufacturing Science and Engineering, 139(5), 051011, 2017. https://doi.org/10.1115/1.4035720

[38] Dumitrache, A., Borangiu T. "IMS10-image-based milling toolpaths with tool engagement control for complex geometry", Engineering Applications of Artificial Intelligence, 25(6), pp. 1161–1172, 2012. https://doi.org/10.1016/j.engappai.2011.09.026

[39] Ochoa González, D. M., Ferreira, J. C. E. "Use of a virtual milling system to generate power-aware tool paths for 2.5-dimensional pocket machining", Proceedings of the Institution of Mechanical Engineers, Part B: Journal of Engineering Manufacture. 2019, 233(13), pp. 2419–2435. https://doi.org/10.1177/0954405419841975

[40] Gasparraj, E. "Constant Material Removal: The Key To Hard Milling", [online] Available at: https://www.mmsonline.com/articles/constant-material-removal-the-key-to-hard-milling [Accessed: 02 June 2025]

[41] Coleman, G. "How to Exceed the Limits of Your Toolpaths", [online] Available at: https://www.moldmakingtechnology.com/articles/how-to-exceed-the-limits-of-your-toolpaths [Accessed: 02 June 2025]

[42] Solidcam "iMachining - The Revolution in CNC Machining", [online] Available at: https://www.solidcam.com/imachining-the-revolution-in-cnc-machining/ [Accessed: 02 June 2025]

[43] Corsi, T. "BoostMilling: comment gagner du temps sur les cycles d'usinage?" (BoostMilling: how to save time on machining cycles?), TopSolid'Blog [online] Available at: https://blog.topsolid.com/fr/boost-milling-gagner-temps-usinage/ [Accessed: 02 June 2025] (in French)

[44] Open Mind Technologies AG "hyperMILL CAD/CAM software, Version 2025", [computer program] Available at: https://www.openmind-tech.com/en/cam/hypermill-2025/ [Accessed: 02 June 2025]

[45] Kollár, J. "Modern nagyoló szerszámpályák II.: A megoldásokat fejlesztők" (Modern roughing tool paths II: Solution developers), [online] Available at: https://www.cnc.hu/2012/07/modern-nagyolo-szerszampalyak-ii-a-megoldasokat-fejlesztok/ [Accessed: 02 June 2025] (in Hungarian)

[46] TRUEMill "TRUEMill - True Engagement Milling", [online] Available at: http://www.truemill.com/content/truemill-true-engagement-milling [Accessed: 02 June 2025]

[47] Coleman, G., Sherbrooke, E. C., Celeritive Technologies, Inc. "High performance milling", US, US8295972B2 (active), 2012. Available at: https://patents.google.com/patent/US8295972B2/en [Accessed: 02. June 2025]

[48] ModuleWorks "High-speed roughing strategy with Adaptive Roughing", [online] Available at: https://www.moduleworks.com/software-components/toolpath/adaptive-roughing/ [Accessed: 02 June 2025]

[49] Berman, M., Osovlanski, D., Calderone, C., Calderone, A., Solidcarn Ltd. "Computerized tool path generation", US, US8489224B2 (active), 2013. Available at: https://patents.google.com/patent/US8489224B2/en?assignee=solidcam&oq=solidcam [Accessed: 02 June 2025]

[50] Ni, B. Y., Elishakoff, I., Jiang, C., Fu, C. M., Han, X. "Generalization of the super ellipsoid concept and its application in mechanics", Applied Mathematical Modelling, 40(21–22), pp. 9427–9444, 2016. https://doi.org/10.1016/j.apm.2016.06.011

[51] Altekin, M., Altay, G. "Static analysis of point-supported super-elliptical plates", Archive of Applied Mechanics, 78(4), pp. 259–266, 2008. https://doi.org/10.1007/s00419-007-0154-9

[52] Bayraktar, H. H., Gupta, A., Kwon, R. Y., Papadopoulos, P., Keaveny, T. M. "The Modified Super-Ellipsoid Yield Criterion for Human Trabecular Bone", Journal of Biomechanical Engineering, 126(6), pp. 677–684, 2005. https://doi.org/10.1115/1.1763177

[53] Rincón-Kohli, L., Zysset, P. K. "Multi-axial mechanical properties of human trabecular bone", Biomechanics and Modeling in Mechanobiology, 8(3), pp. 195–208, 2009. https://doi.org/10.1007/s10237-008-0128-z

[54] Yurdakul, O. C. "Superelliptical extended target tracking with contour measurements", Master Thesis, Middle East Technical University, 2024. [online] Available at: https://open.metu.edu.tr/handle/11511/111009 [Accessed: 02 June 2025]

[55] Shivam, A., Ratnoo, A. "Surveillance Guidance Using Lamé Curve Paths", Journal of Guidance, Control, and Dynamics, 48(5), pp. 1124–1137, 2025. https://doi.org/10.2514/1.G008574

[56] Kohut, P., Miekina, L., Manka, M., Buratowski, T., Klorek, T., Bartkowiak, B. "Measurements of Clothing Circumference Using Vision Methods", In: Solimon, K. S. (ed.) Artificial Intelligence and Machine Learning, Madrid, Spain, 2025, pp. 82–94. ISBN 978-3-031-77493-5 https://doi.org/10.1007/978-3-031-77493-5_9

[57] Tancsa, V., Jacsó, Á., Póka, Gy. "Spiráliszerű szerszámpályák tervezése nagyoló maráshoz Lamé görbék alkalmazásával: Spiral tool path generation for rough milling using Lamé curves", XXXII. Nemzetközi Gépészeti Konferencia – OGÉT 2024, pp. 425–428, 2024.

[58] Jacso, A., Szalay, T., Jauregui, J. C., Resendiz, J. R. "A discrete simulation-based algorithm for the technological investigation of 2.5D milling operations", Proceedings of the Institution of Mechanical Engineers, Part C: Journal of Mechanical Engineering Science, 2018, 233(1), pp. 78–90. https://doi.org/10.1177/0954406218757267